

Polynomially filtered exact diagonalization approach to many-body localization

Piotr Sierant,^{1,2} Maciej Lewenstein,^{2,3} and Jakub Zakrzewski^{1,4}

¹*Institute of Theoretical Physics, Jagiellonian University in Krakow, Łojasiewicza 11, 30-348 Kraków, Poland* *

²*ICFO- Institut de Sciences Fotoniques, The Barcelona Institute of Science and Technology,*

Av. Carl Friedrich Gauss 3, 08860 Castelldefels (Barcelona), Spain

³*ICREA, Pg. Lluís Companys 23, 08010 Barcelona, Spain* †

⁴*Mark Kac Complex Systems Research Center, Jagiellonian University in Krakow, Łojasiewicza 11, 30-348 Kraków, Poland.* ‡

(Dated: September 17, 2020)

Polynomially filtered exact diagonalization method (POLFED) for large sparse matrices is introduced. The algorithm finds an optimal basis of a subspace spanned by eigenvectors with eigenvalues close to a specified energy target by a spectral transformation using a high order polynomial of the matrix. The memory requirements scale better with system size than in the state-of-the-art shift-invert approach. The potential of POLFED is demonstrated examining many-body localization transition in 1D interacting quantum spin-1/2 chains. We investigate the disorder strength and system size scaling of Thouless time. System size dependence of bipartite entanglement entropy and of the gap ratio highlights the importance of finite-size effects. We discuss possible scenarios regarding the many-body localization transition obtaining estimates for the critical disorder strength.

Introduction. Quantum many-body systems are generically expected to approach equilibrium according to eigenstate thermalization hypothesis [1–3]. The phenomenon of many-body localization (MBL) [4–6] provides a robust class of many-body systems which fail to reach thermal equilibrium [7–16]. Further examples of non-ergodic behavior include Stark localization [17, 18], persistent oscillations [19–23], the presence of confinement [24, 25], Hilbert space fragmentation [26–28] or lack of thermalization in lattice gauge theories [29–34].

Classification of many-body systems according to their ergodic properties is a fascinating new direction of research, however, it poses serious technical challenges as exact methods are restricted either to small system sizes [35] or allow to trace time evolution only within a short time interval [36–38]. Hence, a fully consistent theory of MBL transition is missing, with recent approaches pointing towards Kosterlitz-Thouless scaling [39–43]. The finite-size effects strongly influence exact diagonalization (ED) results, leading to a recent debate [44–47] about discriminating between finite size effects and asymptotic features of disordered many-body systems.

The example of MBL transition shows that development of ED techniques allowing to study thermalization properties of possibly large many-body systems is in demand. In this letter, we introduce a polynomially filtered exact diagonalization (POLFED) as a tool to calculate eigenvectors of large sparse matrices with eigenvalues close to a specified energy target. The polynomial spectral transformation preserves the sparse structure of matrices avoiding the main bottleneck of shift-invert method of exact diagonalization (SIMED) [35]. We employ POLFED in study of MBL transition in disordered quantum spin chains unveiling new aspects of system size scaling of Thouless time, entanglement entropy and level statistics. Our results provide novel qualitative and quantitative arguments in favor of the existence of

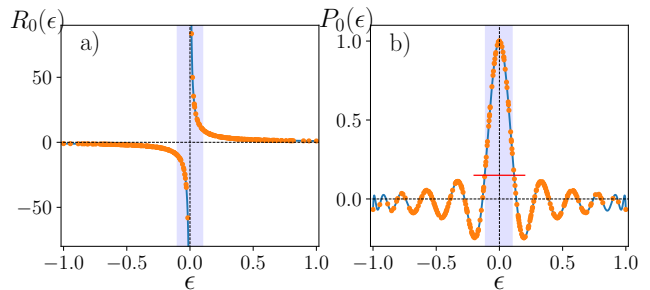


Figure 1. Spectral transformation employed in a) SIMED; b) POLFED algorithm. The spectrum is transformed according to a) $R_0(\epsilon)$; b) $P_{\sigma=0}^{K=22}(\epsilon)$. Eigenvectors corresponding to eigenvalues at the edges of the transformed spectrum (shaded areas) are accessible for iterative methods.

MBL transition in the thermodynamic limit.

Benchmark models. We consider 1D disordered spin chains with Hamiltonian:

$$\hat{H} = \sum_{l=1}^2 \sum_{i=1}^L J_l (S_i^x S_{i+l}^x + S_i^y S_{i+l}^y + \Delta S_i^z S_{i+l}^z) + \sum_{i=1}^L h_i S_i^z, \quad (1)$$

where \vec{S}_i are spin-1/2 matrices, L is the system size, $J_1 = 1$ is fixed as the energy unit, periodic boundary conditions are assumed and $h_i \in [-W, W]$ are independent, uniformly distributed random variables. The XXZ model, widely studied in the MBL context [48–53], is obtained for $J_2 = 0$ and $\Delta = 1$. The choice $J_2 = 1$ and $\Delta = 0.55$ leads to the J_1 - J_2 model studied in [44]. The Hamiltonian (1) becomes a real symmetric sparse matrix $H \in \mathbb{R}^{\mathcal{N} \times \mathcal{N}}$ in basis of eigenstates of S_z^i operator; the matrix size, \mathcal{N} , in the zero magnetization $\sum_i S_i^z = 0$ sector is given by $\mathcal{N} = \binom{L}{L/2} \propto e^{L \ln 2} / \sqrt{L}$.

Calculation of eigenpairs. Hamiltonians of many-body systems are typically characterized by exponential scal-

ing of matrix size, \mathcal{N} , with the system size, L , and sparsity in appropriately chosen basis. For a sparse matrix the number of non-zero entries, N_{nz} , is much smaller than \mathcal{N}^2 implying that matrix vector multiplication requires much less operations than for a dense matrix. The Lanczos algorithm [54] utilizes this fact to find exterior eigenpairs (corresponding to highest/lowest eigenvalues). However, due to an increasing density of states and re-orthogonalization costs, Lanczos algorithm becomes inefficient if many eigenpairs are requested. In contrast, a full ED procedure [55] allows one to determine all eigenpairs of H but, with present day computers, it is limited to $\mathcal{N} \lesssim 5 \cdot 10^4$ corresponding to $L = 18$ in (1). Larger matrix sizes are tractable by SIMED [35]. The Hamiltonian is transformed via $H \rightarrow R_\sigma(H) = (\sigma - H)^{-1}$ so that eigenvalues close to σ become exterior eigenvalues of the matrix $R_\sigma(H)$, see Fig. 1. Consequently, the Lanczos algorithm for the matrix $R_\sigma(H)$ converges to eigenpairs close to the target σ . The Lanczos iteration with $R_\sigma(H)$ is performed by calculating LU decomposition [56, 57] of the matrix H . That has a significant drawback: the sparsity pattern of H is lost resulting in a very severe for large \mathcal{N} phenomenon of fill-in of the matrix. This was identified as the main bottleneck of SIMED when applied to quantum many-body systems [35].

POLFED algorithm. To avoid the fill-in phenomenon and utilize the sparsity of the H matrix in an efficient way, we use the *polynomial spectral transformation*

$$H \rightarrow P_\sigma^K(H) = \frac{1}{D} \sum_{n=0}^K c_n^\sigma T_n(H) \quad (2)$$

where $T_n(x)$ denotes n -th Chebyshev polynomial, the coefficients $c_n^\sigma = \sqrt{4 - 3\delta_{0,n}} \cos(n \arccos \sigma)$ are obtained from expanding a Dirac delta function centered at σ in Chebyshev polynomials and normalization D assures that $P_\sigma(\sigma) = 1$. The eigenvalues close to the target energy σ are the largest eigenvalues of the transformed matrix $P_\sigma(H)$ as shown in Fig. 1b). Hence, a block Lanczos method [58, 59] applied to matrix $P_\sigma^K(H)$ converges to eigenpairs close to the target σ . We note that eigensolvers employing polynomial spectral transformations were considered also in [60–63].

The POLFED consists of the following steps. Lanczos algorithm is used to find the lowest (highest) eigenvalue E_0 (E_1) of matrix H which is then rescaled to $\tilde{H} = [2H - (E_0 + E_1)] / (E_1 - E_0)$. The order K of transformation (2) is specified by requiring that the number of eigenvalues θ_i of $P_\sigma^K(\tilde{H})$ accessible to Lanczos algorithm (belonging to the shaded area in Fig. 1) is equal to a number of requested eigenvalues N_{ev} – as the condition we take $\theta_i \geq p = 0.17$. To find the value of K , an estimate of density of states $\tilde{\rho}(\sigma)$ at energy σ of the matrix \tilde{H} is needed. The $\tilde{\rho}(\sigma)$ can be found efficiently for arbitrary sparse matrices using iterative methods [64, 65]. For the benchmark models (1), the density of states is

Gaussian and is well approximated by an analytic expression $\tilde{\rho}(0) = (E_1 - E_0)\mathcal{N}/\Gamma$ at the center of spectrum $\sigma = 0$ where $\Gamma \propto \sqrt{LW}$. Having found K , the POLFED algorithm, starting with a matrix of orthonormalized random vectors $Q_1 \in \mathbb{R}^{\mathcal{N} \times s}$, performs the block Lanczos iteration

$$U_j = P_\sigma^K(\tilde{H})Q_j - Q_{j-1}B_j^T, \quad A_j = Q_j^T U_j \quad (3)$$

$$R_{j+1} = U_j - Q_j A_j, \quad Q_{j+1} B_{j+1} = R_{j+1}, \quad (4)$$

where $Q_0 = 0$, $B_0 = 0$ and the second operation in (4) is QR decomposition. The iteration is repeated for $j = 1, \dots, m$ resulting in $Q_j, U_j, R_j \in \mathbb{R}^{\mathcal{N} \times s}$ and $A_j, B_j \in \mathbb{R}^{s \times s}$ matrices. In exact arithmetic, columns of Q_j matrices form an orthonormal set of vectors. This property is gradually lost with increasing m during calculations with a finite precision. Hence, between (3) and (4), we perform a re-orthogonalization of columns of matrix U_j against the columns of matrices $\{Q_i\}_{i=1}^j$. The product of $P_\sigma^K(\tilde{H})$ with each column of Q_j in (3) is computed with the Clenshaw algorithm [66]. The orthogonal matrix $\mathcal{Q}_m = [Q_1, \dots, Q_m] \in \mathbb{R}^{\mathcal{N} \times ms}$ defines a block tridiagonal matrix $T_m = \mathcal{Q}_m^T P_\sigma^K(\tilde{H}) \mathcal{Q}_m$ with A_j matrices on the diagonal and B_j (B_j^T) below (above) the diagonal. The eigenvectors $t_i \in \mathbb{R}^{ms}$ of T_m are used to calculate $u_i = \mathcal{Q}_m t_i$ which converge, with increasing m , to exterior eigenvectors of $P_\sigma^K(\tilde{H})$ [67], that is to eigenvectors of \tilde{H} with eigenvalues close to the target σ . The convergence is reached after m steps when the residual norm $\|B_{j+1} \tilde{t}_i\|$ [59] (where \tilde{t}_i are the last s components of the vector t_i and $\|u\| = \sqrt{u^T u}$) vanishes within the numerical precision for each eigenvector t_i corresponding to eigenvalue $\theta_i \geq p$. The eigenvalues of the matrix \tilde{H} are found as $\varepsilon_i = u_i^T \tilde{H} u_i$ and the convergence is verified by a direct calculation of the residual norms $\|\tilde{H} u_i - \varepsilon_i u_i\|$. Each of our tests shows that eigenvalues ε_i are, within numerical precision, equal to N_{ev} eigenvalues of \tilde{H} closest to the target σ . For technical details of the algorithm see [68].

The POLFED is tailored for maximal efficiency in calculations for quantum many-body systems. The order K of the polynomial transformation (2) scales linearly with the density of states $\tilde{\rho}(\sigma)$ that increases exponentially with system size L . Thus, the product $P_\sigma^K(\tilde{H})Q_j$ in (3) is the most time consuming step of the calculation. POLFED offers high scalability as the product can be parallelized in two manners: i) it splits into independent multiplications of subsequent columns of Q_j by $P_\sigma^K(\tilde{H})$; ii) each of the matrix vector multiplications can be parallelized. The re-orthogonalization step between (3) and (4) can be parallelized in a similar manner. The number m of iterations after which the algorithm converges is proportional to N_{ev} . Hence, the memory consumption, dominated by \mathcal{Q}_m , scales as $N_{ev}\mathcal{N}$. The memory requirements of SIMED are larger and scale as $c(L)\mathcal{N}$ where the factor $c(L)$ is due to the fill-in of the matrix. For XXZ model $c(L) \propto 3^{L/2}$ [35]. Moreover, $c(L)$

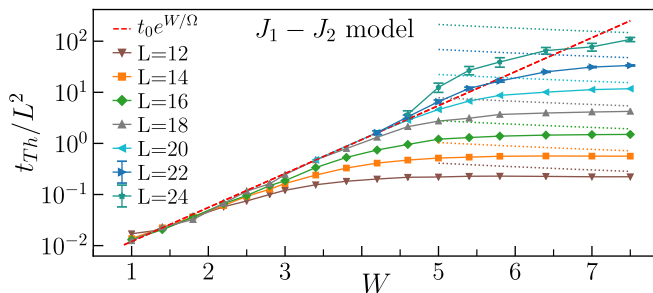


Figure 2. Thouless time t_{Th} for system size L and disorder strength W for J_1 - J_2 model. The dotted lines denote Heisenberg time t_H ; the dashed line denotes a scaling $t_{Th} \propto L^2 e^{W/\Omega}$ broken by the $L = 22, 24$ data.

grows rapidly with number N_{nz} of non-zero elements of the matrix significantly increasing the resources needed in calculations for J_1 - J_2 model. In contrast, computation time of POLFED increases linearly with N_{nz} – resources for XXZ and J_1 - J_2 models are comparable, for detailed benchmarks see [68]. POLFED allows to find larger number of eigenpairs in a single run than the recently proposed eigensolver [69]. This reduces fluctuations of averages over eigenstates and is essential in calculation of the Thouless time.

Thouless time. The spectral form factor is defined as $K(\tau) = \langle |\sum_{j=1}^{\mathcal{N}} g(E_j) e^{-iE_j\tau}|^2 \rangle / Z$, where E_j are eigenvalues of H after an unfolding procedure [70], $g(\epsilon)$ is a Gaussian function, the average is taken over disorder realizations and Z is a normalization constant assuring $K(\tau) \xrightarrow{\tau \rightarrow \infty} 1$. The spectral form factor of many-body system (with time reversal invariance) follows Gaussian Orthogonal Ensemble (GOE) prediction $K(\tau) = K_{GOE}(\tau)$ only for $\tau > \tau_{Th}$ defining the Thouless time $t_{Th} = \tau_{Th} t_H$, where $t_H = 2\pi\rho(0)$ is the Heisenberg time.

The Thouless time, t_{Th} , calculated for J_1 - J_2 spin chains of length $L \leq 18$ [44] scales as $t_{Th} \propto L^2 e^{W/\Omega}$ where W is the disorder strength and Ω is constant. If this scaling prevailed in $L \rightarrow \infty$ limit, it would imply $t_{Th}/t_H \rightarrow 0$ so that the system would be well described by GOE and MBL phase would be absent for arbitrary disorder strength in the thermodynamic limit. To verify this surprising conclusion we supplement results of full ED of J_1 - J_2 model with Thouless times obtained with POLFED for $L = 20, 22, 24$ respectively for 800, 200, 50 disorder realizations. Since we calculate $N_{ev} = 2500$ eigenvalues in the middle of spectrum ($\sigma = 0$), the sum in the definition of spectral form factor $K(\tau)$ is truncated. However, this does not influence the value of t_{Th} as long as it is larger than a certain threshold value determined by N_{ev} [68]. The obtained Thouless times are shown in Fig. 2. Data for $L \leq 20$ follows the scaling $t_{Th} \propto L^2 e^{W/\Omega}$ deviating from it at disorder strength $\tilde{W}(L)$ which increases with the system size, for instance $\tilde{W}(18) \approx 3.7$ or $\tilde{W}(20) \approx 4.6$. This behavior changes qualitatively for

$L = 22, 24$ data breaking the scaling $t_{Th} \propto L^2 e^{W/\Omega}$. Similar behavior heralds Anderson localization transition in single particle disordered systems [45], hence, our data suggest the presence of the transition to MBL phase in J_1 - J_2 model. Therefore, one has to reach a sufficiently large L to see the correct scaling of Thouless time, which raises the question about the finite size effects at MBL transition.

Entanglement entropy and level statistics. The entanglement entropy allows for insights in nature of MBL transition [71–73]. The entanglement entropy of an eigenstate is defined as $S_E = -\sum_i \alpha_i^2 \log(\alpha_i^2)$, where α_i are Schmidt basis coefficients (see e.g. [74]) associated with the bipartition of the lattice into subsystems containing sites $[x, x + L/2)$ and $[x + L/2, x + L)$ (the sites are numbered modulo L). We average S_E over the position of the cut x , over $N_{ev} \leq \min\{\mathcal{N}/100, 2000\}$ eigenstates in the middle of the spectrum ($\sigma = 0$) of J_1 - J_2 model for system sizes $12 \leq L \leq 24$ (for $L = 8, 10$ we take $N_{ev} = 5$) as well as over more than 5000, 200, 50 disorder realizations respectively for $L \leq 20$, $L = 22$, $L = 24$. Finally, we obtain the scaled entanglement entropy $s_E = S_E/S_{RMT}(L)$ where $S_{RMT}(L) = (L/2) \ln(2) + (1/2 + \ln(1/2))/2 - 1/2$ corresponds to a chaotic spin chain in the total $\sum_i S_i^z = 0$ sector [75]. The resulting s_E is shown in Fig. 3a). For available system sizes, the scaled entanglement entropy s_E : i) monotonically increases with L for $W \lesssim 3.4$; ii) monotonically decreases for $W \gtrsim 11$; iii) decreases for smaller L and starts increasing for larger system sizes (a similar reentrant behavior was observed e.g. in [47, 76]). The behavior i) clearly leads to an ergodic system at large L . In contrast, for large disorder strengths e.g. $W = 15$, an area law of entanglement entropy [77, 78] $s_E \propto 1/L$ arises due to the emergent integrability of MBL phase [79–85]. Averaging $r_i = \min\{g_i, g_{i+1}\} / \max\{g_i, g_{i+1}\}$ (where $g_i = E_{i+1} - E_i$) over eigenvalues corresponding to eigenstates from which s_E was calculated, we obtain a mean gap ratio \bar{r} shown in Fig. 3b). The mean gap ratio \bar{r} probes level statistics of the system, admitting values characteristic for GOE and Poisson statistics for ergodic and localized systems [7, 86]. Similarly as for s_E , the mean gap ratio \bar{r} follows the three types of behavior with system size depending on disorder strength W .

To understand whether and at which disorder strength the MBL transition takes place one has to study the interplay between the ii) and iii) trends. To this end, we find the disorder strength $W_E^*(L)$ such that $s_E(L-1) = s_E(L+1)$ for odd L and $s_E(L-2) = s_E(L+2)$ for even L , for details see [68]. Smooth changes of s_E with L and W assure that $W_E^*(L)$ is the largest disorder strength, for a given system size L , at which the volume-law $S_E \propto L$, expected for an ergodic system, is still obeyed. Consequently, the disorder strength $W_E^*(L)$ is a lower bound for the critical disorder strength W_C of the transition to MBL phase. Fig. 3c) shows the relation between W_E^* and $1/L$ along with disorder strength $W_{\bar{r}}^*$ obtained in

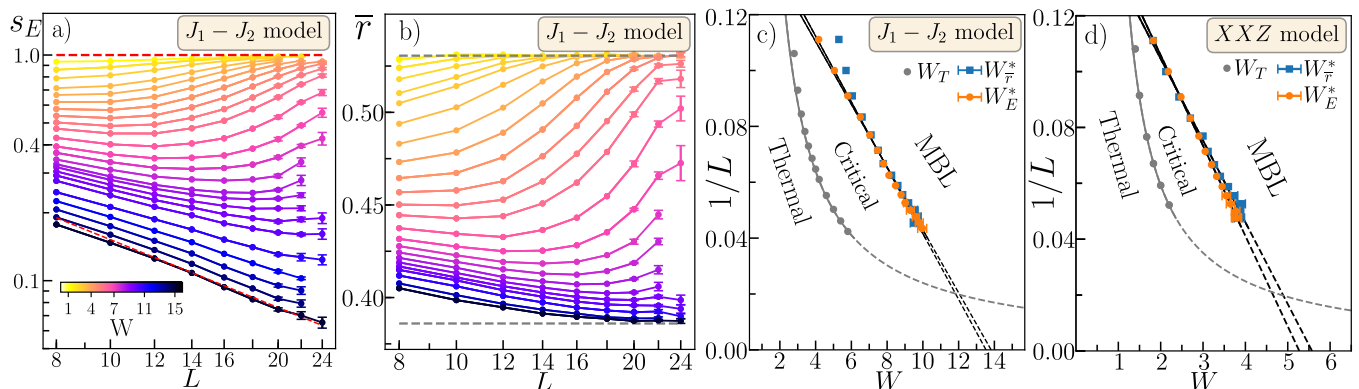


Figure 3. Finite size effects at MBL transition. a) The entanglement entropy s_E of eigenstates of J_1 - J_2 model vs system size L for disorder strengths $W = 1.4, \dots, 15$ (denoted on the color bar), dashed lines correspond to ergodic and MBL behavior; b) the same for the gap ratio \bar{r} , dashed lines correspond to GOE and Poisson limits; c) $W_{E,\bar{r}}^*$ and W_T as function $1/L$ for J_1 - J_2 model (see text); d) the same for XXZ model.

analogous manner for the average gap ratio \bar{r} . Another aspect of finite size effects at MBL transition is revealed when, for given L , one finds a disorder strength $W_T(L)$ for which the scaled entanglement entropy is close to the ergodic limit, e.g. $s_E(W_T) = 0.8$. Such a criterion yields $W_T \propto L$. Equivalently, W_T can be found as a disorder strength for which the average gap ratio \bar{r} departs from the GOE limit [44]. This allows us to identify the following regimes: A) thermal, for $W < W_T$, with entanglement entropy fulfilling the volume-law and close to the value for chaotic spin chain $s_E \approx S_{RMT}(L)$ and level statistics well described by GOE; B) critical, for $W_{E,\bar{r}}^* < W < W_T$, with $s_E < S_{RMT}(L)$ but scaling super linearly with L and value of \bar{r} increasing with L towards the GOE limit; C) MBL, for $W < W_{E,\bar{r}}^*$, with both scaled entanglement entropy $s_E(L)$ and average gap ratio \bar{r} decreasing with system size L . Fig. 3d) shows that behavior of the XXZ model is similar (data for s_E and \bar{r} can be found in [68]). The three regimes resemble the qualitative picture of MBL transition proposed in [73].

The asymptotic features of disordered spin chains depend on how $W_{E,\bar{r}}^*$ and W_T behave in thermodynamic limit. For available system sizes, $8 \leq L \leq 24$, the linear scaling of W_T with L as well as the linear scaling of $W_{E,\bar{r}}^*$ with inverse of system size $1/L$, denoted by solid lines in Fig. 3 c), d), are accurately obeyed. Extrapolating the scalings (dashed lines in the same Fig.), leads to the crossing $W_T = W_{E,\bar{r}}^*$ at $L_0 \approx 50$ showing the incompatibility of the two scalings. Thus, it seems conceivable that studying eigenstates at system size L_0 would yield conclusive results about the $L \rightarrow \infty$ limit, c.f. [47]. However, it is also possible that either of the scalings breaks down at smaller L achievable in the near future with POLFED.

The unveiled linear dependence of $W_{E,\bar{r}}^*$ on $1/L$ is consistently approached by data for all system sizes. Extrapolating to $L \rightarrow \infty$ limit, we get estimates of critical

disorder strength

$$W_C^{J_1-J_2} \approx 13.7 \quad \text{and} \quad W_C^{XXZ} \approx 5.4, \quad (5)$$

respectively for J_1 - J_2 and XXZ models. Our estimate for W_C^{XXZ} is larger than the value $W_C \approx 3.7$ for XXZ model [87] (which yields the critical exponent violating the Harris criterion [88–90]) or the estimates obtained after an asymmetric scalings on both sides of the transition: $W_C \approx 3.8$ [91], $W_C \approx 4.2$ [42]. Since our approach relies on an analysis of the drift of crossing points of $s_E(W)$ and $\bar{r}(W)$ curves, it does not rely on any finite size scaling procedure. Our estimate for W_C^{XXZ} is consistent with the lower bound $W_C > 4.5$ of [92] as well as with $W_C > 5$ obtained in analysis of quench dynamics of large XXZ spin chain [37].

Conclusions. The POLFED algorithm, thanks to the employed polynomial spectral transformation, has a better scaling of computation time with matrix size \mathcal{N} than the state-of-the-art SIMED algorithm. Avoiding the fill-in phenomenon, POLFED has a significantly lower memory consumption than SIMED, moreover, its performance decreases only linearly with increasing the number of non-zero off-diagonal matrix entries. For those reasons POLFED opens new pathways in studies of highly excited states of many-body systems with potential applications to systems with long-range interactions realized in experiments with polar molecules [93], Rydberg atoms [94], trapped ions [95–97] and problems of MBL or information spreading in the presence of power-law interactions [98–117]. Understanding the relation of POLFED to alternative eigensolvers [69, 118, 119] is an interesting task for a further research.

POLFED allowed us to study MBL transition in J_1 - J_2 model of size $L \leq 24$. Such a system size is sufficient to demonstrate the breakdown of the scaling $t_{Th} \propto L^2 e^{W/\Omega}$ of Thouless time [44]. Studying the system size scaling of entanglement entropy s_E of eigenstates we estimated the critical disorder strength of transition to MBL phase.

Acknowledgments. We thank Fabien Alet and Dominique Delande for insightful discussions. The computations have been performed within PL-Grid infrastructure, its support is acknowledged. M.L. acknowledges the Spanish Ministry MINECO (National Plan 15 Grant: FISICATEAMO No. FIS2016-79508-P, SEVERO OCHOA No. SEV-2015-0522, FPI), European Social Fund, Fundació Cellex, Fundació Mir-Puig, Generalitat de Catalunya (AGAUR Grant No. 2017 SGR 1341, CERCA/Program), ERC AdG NOQIA, EU FEDER, MINECO-EU QUANTERA MAQS (funded by The State Research Agency (AEI) PCI2019-111828-2 / 10.13039/501100011033), and the National Science Centre, Poland-Symfonia Grant No. 2016/20/W/ST4/00314. The support of National Science Centre, Poland under Unisono Grant No. 2017/25/Z/ST2/03029 (Quantero: QTFLAG) is also acknowledged (J.Z.). P.S. acknowledges National Science Centre, Poland: ETIUDA grant No. 2018/28/T/ST2/00401.

* piotr.sierant@uj.edu.pl

† maciej.lewenstein@icfo.eu

‡ jakub.zakrzewski@uj.edu.pl

- [1] J. M. Deutsch, *Phys. Rev. A* **43**, 2046 (1991).
- [2] M. Srednicki, *Phys. Rev. E* **50**, 888 (1994).
- [3] L. D'Alessio, Y. Kafri, A. Polkovnikov, and M. Rigol, *Advances in Physics* **65**, 239 (2016), <https://doi.org/10.1080/00018732.2016.1198134>.
- [4] R. Nandkishore and D. A. Huse, *Ann. Rev. Cond. Mat. Phys.* **6**, 15 (2015).
- [5] F. Alet and N. Laflorencie, *Comptes Rendus Physique* **19**, 498 (2018).
- [6] D. A. Abanin, E. Altman, I. Bloch, and M. Serbyn, *Rev. Mod. Phys.* **91**, 021001 (2019).
- [7] V. Oganesyan and D. A. Huse, *Phys. Rev. B* **75**, 155111 (2007).
- [8] A. Pal and D. A. Huse, *Phys. Rev. B* **82**, 174411 (2010).
- [9] J. A. Kjäll, J. H. Bardarson, and F. Pollmann, *Phys. Rev. Lett.* **113**, 107204 (2014).
- [10] Y. Bar Lev, D. R. Reichman, and Y. Sagi, *Phys. Rev. B* **94**, 201116 (2016).
- [11] R. Mondaini and M. Rigol, *Phys. Rev. A* **92**, 041601 (2015).
- [12] P. Prelovšek, O. S. Barišić, and M. Žnidarič, *Phys. Rev. B* **94**, 241104 (2016).
- [13] P. Sierant, D. Delande, and J. Zakrzewski, *Phys. Rev. A* **95**, 021601 (2017).
- [14] M. Kozarzewski, P. Prelovšek, and M. Mierzejewski, *Phys. Rev. Lett.* **120**, 246602 (2018).
- [15] P. Sierant and J. Zakrzewski, *New Journal of Physics* **20**, 043032 (2018).
- [16] N. Macé, N. Laflorencie, and F. Alet, *SciPost Phys.* **6**, 50 (2019).
- [17] M. Schulz, C. A. Hooley, R. Moessner, and F. Pollmann, *Phys. Rev. Lett.* **122**, 040606 (2019).
- [18] E. van Nieuwenburg, Y. Baum, and G. Refael, *Proceedings of the National Academy of Sciences* **116**, 9269 (2019).
- [19] C. J. Turner, A. A. Michailidis, D. A. Abanin, M. Serbyn, and Z. Papić, *Nature Physics* **14**, 745–749 (2018).
- [20] W. W. Ho, S. Choi, H. Pichler, and M. D. Lukin, *Phys. Rev. Lett.* **122**, 040603 (2019).
- [21] V. Khemani, C. R. Laumann, and A. Chandran, *Physical Review B* **99**, 161101 (2019).
- [22] T. Iadecola and M. Žnidarič, *Phys. Rev. Lett.* **123**, 036403 (2019).
- [23] M. Schecter and T. Iadecola, *Phys. Rev. Lett.* **123**, 147201 (2019).
- [24] A. J. A. James, R. M. Konik, and N. J. Robinson, *Phys. Rev. Lett.* **122**, 130603 (2019).
- [25] T. Chanda, R. Yao, and J. Zakrzewski, *Phys. Rev. Research* **2**, 032039 (2020).
- [26] P. Sala, T. Rakovszky, R. Verresen, M. Knap, and F. Pollmann, *Physical Review X* **10** (2020), [10.1103/physrevx.10.011047](https://doi.org/10.1103/physrevx.10.011047).
- [27] V. Khemani, M. Hermele, and R. Nandkishore, *Phys. Rev. B* **101**, 174204 (2020).
- [28] T. Rakovszky, P. Sala, R. Verresen, M. Knap, and F. Pollmann, *Phys. Rev. B* **101**, 125126 (2020).
- [29] A. Smith, J. Knolle, R. Moessner, and D. L. Kovrizhin, *Phys. Rev. Lett.* **119**, 176601 (2017).
- [30] M. Brenes, M. Dalmonte, M. Heyl, and A. Scardicchio, *Phys. Rev. Lett.* **120**, 030601 (2018).
- [31] G. Magnifico, M. Dalmonte, P. Facchi, S. Pascazio, F. V. Pepe, and E. Ercolessi, *Quantum* **4**, 281 (2020).
- [32] T. Chanda, J. Zakrzewski, M. Lewenstein, and L. Tagliacozzo, *Phys. Rev. Lett.* **124**, 180602 (2020).
- [33] G. Giudici, F. M. Surace, J. E. Ebot, A. Scardicchio, and M. Dalmonte, *Phys. Rev. Research* **2**, 032034 (2020).
- [34] F. M. Surace, P. P. Mazza, G. Giudici, A. Leroze, A. Gambassi, and M. Dalmonte, *Phys. Rev. X* **10**, 021041 (2020).
- [35] F. Pietracaprina, N. Macé, D. J. Luitz, and F. Alet, *SciPost Phys.* **5**, 45 (2018).
- [36] T. Enss, F. Andraschko, and J. Sirker, *Phys. Rev. B* **95**, 045121 (2017).
- [37] E. V. H. Doggen, F. Schindler, K. S. Tikhonov, A. D. Mirlin, T. Neupert, D. G. Polyakov, and I. V. Gornyi, *Phys. Rev. B* **98**, 174202 (2018).
- [38] T. Chanda, P. Sierant, and J. Zakrzewski, *Phys. Rev. B* **101**, 035148 (2020).
- [39] A. Goremykina, R. Vasseur, and M. Serbyn, *Phys. Rev. Lett.* **122**, 040601 (2019).
- [40] A. Morningstar and D. A. Huse, *Phys. Rev. B* **99**, 224205 (2019).
- [41] P. T. Dumitrescu, A. Goremykina, S. A. Parameswaran, M. Serbyn, and R. Vasseur, *Phys. Rev. B* **99**, 094205 (2019).
- [42] N. Laflorencie, G. Lemarié, and N. Macé, “Chain breaking and Kosterlitz-Thouless scaling at the many-body localization transition,” (2020), [arXiv:2004.02861](https://arxiv.org/abs/2004.02861).
- [43] J. Šuntajs, J. Bonča, T. Prosen, and L. Vidmar, *Phys. Rev. B* **102**, 064207 (2020).
- [44] J. Šuntajs, J. Bonča, T. Prosen, and L. Vidmar, (2019), [arXiv:1905.06345](https://arxiv.org/abs/1905.06345).
- [45] P. Sierant, D. Delande, and J. Zakrzewski, *Phys. Rev. Lett.* **124**, 186601 (2020).
- [46] D. A. Abanin, J. H. Bardarson, G. D. Tomasi, S. Gopalakrishnan, V. Khemani, S. A. Parameswaran, F. Pollmann, A. C. Potter, M. Serbyn, and R. Vasseur,

- (2019), [arXiv:1911.04501](https://arxiv.org/abs/1911.04501).
- [47] R. K. Panda, A. Scardicchio, M. Schulz, S. R. Taylor, and M. Žnidarič, *EPL (Europhysics Letters)* **128**, 67003 (2020).
- [48] K. Agarwal, S. Gopalakrishnan, M. Knap, M. Müller, and E. Demler, *Phys. Rev. Lett.* **114**, 160401 (2015).
- [49] S. Bera, H. Schomerus, F. Heidrich-Meisner, and J. H. Bardarson, *Phys. Rev. Lett.* **115**, 046603 (2015).
- [50] S. Bera, G. De Tomasi, F. Weiner, and F. Evers, *Phys. Rev. Lett.* **118**, 196801 (2017).
- [51] L. Herviou, S. Bera, and J. H. Bardarson, *Phys. Rev. B* **99**, 134205 (2019).
- [52] L. Colmenarez, P. A. McClarty, M. Haque, and D. J. Luitz, (2019), [arXiv:1906.10701](https://arxiv.org/abs/1906.10701).
- [53] P. Sierant and J. Zakrzewski, *Phys. Rev. B* **101**, 104201 (2020).
- [54] C. Lanczos, *Journal of Research of the National Bureau of Standards* **45** (1950).
- [55] G. H. Golub and C. F. Van Loan, *Matrix computations*, Vol. 3 (JHU press, 2012).
- [56] P. R. Amestoy, I. S. Duff, J.-Y. L'Excellent, and J. Koster, *SIAM Journal on Matrix Analysis and Applications* **23**, 15 (2001).
- [57] P. R. Amestoy, A. Guermouche, J.-Y. L'Excellent, and S. Pralet, *Parallel Computing* **32**, 136 (2006), parallel Matrix Algorithms and Applications (PMAA'04).
- [58] J. Cullum and W. E. Donath, in *1974 IEEE Conference on Decision and Control including the 13th Symposium on Adaptive Processes* (IEEE, 1974) pp. 505–509.
- [59] G. Golub and R. Underwood, in *Mathematical Software*, edited by J. R. Rice (Academic Press, 1977) pp. 361 – 377.
- [60] C. Bekas, E. Kokiopoulou, and Y. Saad, *SIAM Journal on Matrix Analysis and Applications* **30**, 397 (2008).
- [61] H.-R. Fang and Y. Saad, *SIAM Journal on Scientific Computing* **34**, A2220 (2012).
- [62] R. Li, Y. Xi, E. Vecharynski, C. Yang, and Y. Saad, *SIAM Journal on Scientific Computing* **38**, A2512 (2016).
- [63] A. Pieper, M. Kreutzer, A. Alvermann, M. Galgon, H. Fehske, G. Hager, B. Lang, and G. Wellein, *Journal of Computational Physics* **325**, 226 (2016).
- [64] R. Silver and H. Röder, *International Journal of Modern Physics C* **05**, 735 (1994).
- [65] R. Silver, H. Roeder, A. Voter, and J. Kress, *Journal of Computational Physics* **124**, 115 (1996).
- [66] C. W. Clenshaw, *Mathematics of Computation* **9**, 118 (1955).
- [67] Y. Saad, *SIAM Journal on Numerical Analysis* **17**, 687 (1980).
- [68] See Supplemental Material at [URL will be inserted by publisher].
- [69] R. Van Beeumen, G. D. Kahanamoku-Meyer, N. Y. Yao, and C. Yang, in *Proceedings of the International Conference on High Performance Computing in Asia-Pacific Region* (2020) pp. 179–187.
- [70] J. M. G. Gómez, R. A. Molina, A. Relaño, and J. Retamosa, *Phys. Rev. E* **66**, 036209 (2002).
- [71] X. Yu, D. J. Luitz, and B. K. Clark, *Phys. Rev. B* **94**, 184202 (2016).
- [72] V. Khemani, D. N. Sheng, and D. A. Huse, *Phys. Rev. Lett.* **119**, 075702 (2017).
- [73] V. Khemani, S. P. Lim, D. N. Sheng, and D. A. Huse, *Phys. Rev. X* **7**, 021013 (2017).
- [74] I. Bengtsson and K. Życzkowski, *Geometry of Quantum States: An Introduction to Quantum Entanglement* (Cambridge University Press, 2006).
- [75] L. Vidmar and M. Rigol, *Phys. Rev. Lett.* **119**, 220603 (2017).
- [76] M. Serbyn, Z. Papić, and D. A. Abanin, *Phys. Rev. X* **5**, 041047 (2015).
- [77] B. Bauer and C. Nayak, *Journal of Statistical Mechanics: Theory and Experiment* **2013**, P09005 (2013).
- [78] M. Serbyn, Z. Papić, and D. A. Abanin, *Phys. Rev. Lett.* **110**, 260601 (2013).
- [79] M. Serbyn, Z. Papić, and D. A. Abanin, *Phys. Rev. Lett.* **111**, 127201 (2013).
- [80] D. A. Huse, R. Nandkishore, and V. Oganesyan, *Phys. Rev. B* **90**, 174202 (2014).
- [81] V. Ros, M. Mueller, and A. Scardicchio, *Nuclear Physics B* **891**, 420 (2015).
- [82] J. Z. Imbrie, *Phys. Rev. Lett.* **117**, 027201 (2016).
- [83] T. B. Wahl, A. Pal, and S. H. Simon, *Phys. Rev. X* **7**, 021018 (2017).
- [84] M. Mierzejewski, M. Kozarzewski, and P. Prelovšek, *Phys. Rev. B* **97**, 064204 (2018).
- [85] S. J. Thomson and M. Schiró, *Phys. Rev. B* **97**, 060201 (2018).
- [86] Y. Y. Atas, E. Bogomolny, O. Giraud, and G. Roux, *Phys. Rev. Lett.* **110**, 084101 (2013).
- [87] D. J. Luitz, N. Laflorencie, and F. Alet, *Phys. Rev. B* **91**, 081103 (2015).
- [88] A. B. Harris, *Journal of Physics C: Solid State Physics* **7**, 1671 (1974).
- [89] J. T. Chayes, L. Chayes, D. S. Fisher, and T. Spencer, *Phys. Rev. Lett.* **57**, 2999 (1986).
- [90] A. Chandran, C. R. Laumann, and V. Oganesyan, (2015), [arXiv:1509.04285](https://arxiv.org/abs/1509.04285).
- [91] N. Macé, F. Alet, and N. Laflorencie, *Phys. Rev. Lett.* **123**, 180601 (2019).
- [92] T. Devakul and R. R. P. Singh, *Phys. Rev. Lett.* **115**, 187201 (2015).
- [93] B. Yan, S. A. Moses, B. Gadway, J. P. Covey, K. R. A. Hazzard, A. M. Rey, D. S. Jin, and J. Ye, *Nature* **501**, 521 (2013).
- [94] A. Browaeys and T. Lahaye, *Nature Physics* **16**, 132 (2020).
- [95] P. Richerme, Z.-X. Gong, A. Lee, C. Senko, J. Smith, M. Foss-Feig, S. Michalakis, A. V. Gorshkov, and C. Monroe, *Nature* **511**, 198 (2014).
- [96] P. Jurcevic, B. P. Lanyon, P. Hauke, C. Hempel, P. Zoller, R. Blatt, and C. F. Roos, *Nature* **511**, 202 (2014).
- [97] J. Smith, A. Lee, P. Richerme, B. Neyenhuis, P. W. Hess, P. Hauke, M. Heyl, D. A. Huse, and C. Monroe, *Nature Physics* **12**, 907 (2016).
- [98] A. L. Burin, “Energy delocalization in strongly disordered systems induced by the long-range many-body interaction,” (2006), [arXiv:cond-mat/0611387](https://arxiv.org/abs/cond-mat/0611387) [cond-mat.dis-nn].
- [99] N. Y. Yao, C. R. Laumann, S. Gopalakrishnan, M. Knap, M. Müller, E. A. Demler, and M. D. Lukin, *Phys. Rev. Lett.* **113**, 243002 (2014).
- [100] A. L. Burin, *Phys. Rev. B* **91**, 094202 (2015).
- [101] P. Hauke and M. Heyl, *Phys. Rev. B* **92**, 134204 (2015).
- [102] H. Li, J. Wang, X.-J. Liu, and H. Hu, *Phys. Rev. A* **94**, 063625 (2016).
- [103] D. B. Gutman, I. V. Protopopov, A. L. Burin, I. V.

- Gornyi, R. A. Santos, and A. D. Mirlin, *Phys. Rev. B* **93**, 245427 (2016).
- [104] R. Singh, R. Moessner, and D. Roy, *Phys. Rev. B* **95**, 094205 (2017).
- [105] R. M. Nandkishore and S. L. Sondhi, *Phys. Rev. X* **7**, 041021 (2017).
- [106] K. S. Tikhonov and A. D. Mirlin, *Phys. Rev. B* **97**, 214205 (2018).
- [107] A. Safavi-Naini, M. L. Wall, O. L. Acevedo, A. M. Rey, and R. M. Nandkishore, *Phys. Rev. A* **99**, 033610 (2019).
- [108] G. De Tomasi, *Phys. Rev. B* **99**, 054204 (2019).
- [109] T. Botzung, D. Vodola, P. Naldesi, M. Müller, E. Ercolessi, and G. Pupillo, *Phys. Rev. B* **100**, 155136 (2019).
- [110] S. Roy and D. E. Logan, *SciPost Phys.* **7**, 42 (2019).
- [111] S. Schiffer, J. Wang, X.-J. Liu, and H. Hu, *Phys. Rev. A* **100**, 063619 (2019).
- [112] S. Nag and A. Garg, *Phys. Rev. B* **99**, 224203 (2019).
- [113] B. Kloss and Y. Bar Lev, *Phys. Rev. B* **102**, 060201 (2020).
- [114] X. Deng, G. Masella, G. Pupillo, and L. Santos, *Phys. Rev. Lett.* **125**, 010401 (2020).
- [115] D. J. Luitz and Y. Bar Lev, *Phys. Rev. A* **99**, 010105 (2019).
- [116] C.-F. Chen and A. Lucas, *Phys. Rev. Lett.* **123**, 250605 (2019).
- [117] A. Y. Guo, M. C. Tran, A. M. Childs, A. V. Gorshkov, and Z.-X. Gong, *Phys. Rev. A* **102**, 010401 (2020).
- [118] M. Bollhöfer and Y. Notay, *Computer Physics Communications* **177**, 951 (2007).
- [119] E. Polizzi, *Phys. Rev. B* **79**, 115112 (2009).
- [120] N. Bell and M. Garland, *Efficient sparse matrix-vector multiplication on CUDA*, Tech. Rep. (2008).
- [121] S. Acer, O. Selvitopi, and C. Aykanat, *Parallel Computing* **59**, 71 (2016).
- [122] S. Chen, J. Fang, D. Chen, C. Xu, and Z. Wang, arXiv preprint arXiv:1805.11938 (2018).
- [123] H. A. H. Baca and F. de Luz Palomino Valdivia, in *2019 IEEE XXVI International Conference on Electronics, Electrical Engineering and Computing (INTERCON)* (2019) pp. 1–4.

SUPPLEMENTARY MATERIAL

Convergence of POLFED

POLFED performs the iteration of the block Lanczos method for the transformed matrix $P_\sigma^K(\tilde{H})$ until all of the residual norms associated with eigenvalues $\theta_i \geq p = 0.17$ vanish within numerical precision. Fig. 4 shows the number n_{ev} of converged (with the vanishing residual norm) eigenpairs in few runs of POLFED. Re-

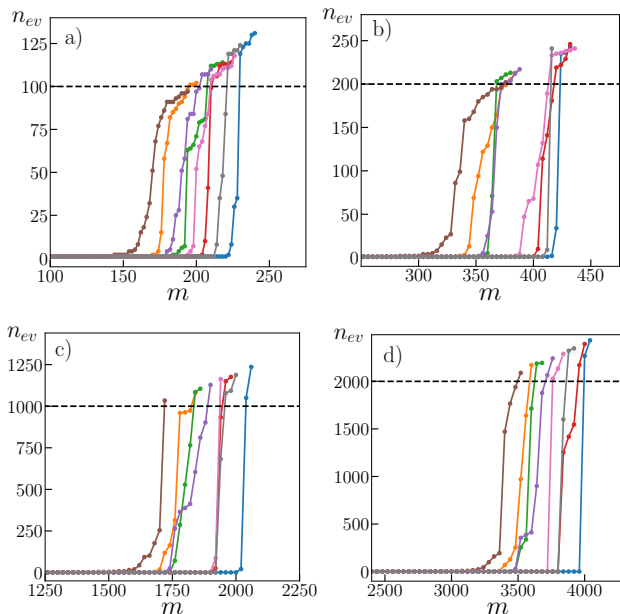


Figure 4. Convergence of POLFED. Number of converged eigenpairs n_{ev} as a function of number of Lanczos steps m . Dotted lines correspond to 8 different disorder realizations with disorder strength $W = 5.4$ for J_1 - J_2 model, system size is $L = 20$. The block size $s = 1$. Panels a), b), c) and d) correspond, respectively, to the number of requested eigenvalues $N_{ev} = 100, 200, 1000, 2000$ (denoted by black dashed lines).

gardless of the number N_{ev} of requested eigenvalues, n_{ev} increases rapidly, once the number m of Lanczos steps exceeds a certain threshold value which is typically twice larger than N_{ev} . Therefore, the eigenpairs start to converge only when the \mathcal{Q}_m matrix contains the full basis of subspace of Hilbert space spanned by eigenvectors with eigenvalues close to the energy σ . It is beneficial to stop the algorithm once $n_{ev} \geq N_{ev}$. Further increase of m does not lead to an increase in n_{ev} because of the large density of states of $P_\sigma^K(\tilde{H})$ close to $\theta \approx 0.15$ due to the the secondary minima of $P_\sigma^K(\epsilon)$ (see Fig. 1 of the main text).

POLFED follows the convergence pattern described above provided that the polynomial spectral transformation P_σ^K (in particular, its order K) is chosen in such a way that the number N_{ev} of requested eigenvalues corresponds to the number n_P of eigenvalues of $P_\sigma^K(\tilde{H})$ that

are accessible to the method (i.e. fulfill the $\theta > p = 0.17$ condition). To calculate n_P , POLFED uses the function $P_\sigma^K(\epsilon)$ as well as the density of states of the \tilde{H} . As the density of states in the middle of the spectrum of the benchmark models considered in this work we use an analytical expression $\tilde{\rho}(0) = (E_1 - E_0)\mathcal{N}/\Gamma$, where

$$\Gamma = \sqrt{L[(1 + J_2^2)/8 + \Delta^2(1 + J_2^2)/16 + W^2/12]}, \quad (6)$$

as obtained in [44]. The fluctuations of density of states between disorder realizations lead to the fluctuations of the threshold value of m beyond which the convergence occurs – see Fig. 4. Those fluctuations are enhanced when disorder strength increases. However, our tests indicate that the convergence occurs for each of the considered disorder values ($W \leq 15$) and disorder realizations for $m < 2.8N_{ev}$.

Testing a variety of the polynomial spectral transformation $P_\sigma^K(\tilde{H})$ as well as different stopping criteria, we checked that POLFED allows to minimize the time of calculation until the convergence is reached and, at the same time, allows to keep a relatively large the total number of eigenpairs obtained in a single run.

When the block size s of the Lanczos method is increased, the total number of vectors generated in the iteration, ms , required for the convergence of algorithm, is also increased. However, for the typical production runs done in this work, i.e. with the block size $s \leq 24$ and $N_{ev} \geq 1000$, the total number of Lanczos vectors still fulfills the condition $ms < 2.8N_{ev}$. Thus, during its start, POLFED allocates $2.8N_{ev}$ columns of the matrix \mathcal{Q}_m . The associated memory consumption is proportional to $N_{ev}\mathcal{N}$, which has the dominant contribution to total memory occupation of POLFED.

Technical details of POLFED

Calculation of the product of $P_\sigma^K(\tilde{H})$ with subsequent columns of Q_j is the most time consuming step of POLFED. The recurrence relation $T_{n+2}(x) = 2xT_{n+1}(x) - T_n(x)$ fulfilled by Chebyshev polynomials reduces this product to multiplication of vectors by the sparse matrix \tilde{H} and basic linear algebra operations. The Clenshaw algorithm [66], allows us to reduce the number operations needed to calculate the product.

The efficiency of computation of $P_\sigma^K(\tilde{H})x$ where $x \in \mathbb{R}^{\mathcal{N}}$ is crucially dependent on efficiency of the single sparse matrix vector multiplication $\tilde{H}x$. In the current version of POLFED we store the \tilde{H} matrix in CSR format. We do not store the off-diagonal Hamiltonian entries of H as they are all equal to $H_{ij} = 1/2$. On one hand this reduces the memory consumption associated with storing of the Hamiltonian matrix. On the other hand, POLFED does not access the values of H_{ij} during the matrix-vector multiplication which increases

the efficiency of the code. Throughout this work, we consider block sizes $s \leq 24$ calculating the products of $P_\sigma^K(\tilde{H})$ with columns of matrix Q_j independently. Each of the products is calculated on a single core. Effectively, POLFED performs the computation in parallel on s cores. The re-orthogonalization of columns of matrix U_j obtained in Lanczos step against the columns of matrices $\{Q_i\}_{i=1}^j$ is parallelized similarly: each of the s cores orthogonalizes a single column of U_j against the columns of $\{Q_i\}_{i=1}^j$.

The matrix-vector multiplications $\tilde{H}x$ could be performed on multiple cores with use of external sparse basic linear algebra libraries, resulting in higher degree of parallelism in POLFED. Moreover, the promising way of enhancing the performance of POLFED is to optimize the sparse matrix-vector product, a subject that recently received attention both on CPUs as well as on GPUs [120–123].

Benchmark for disorder spin chains

In this section we compare performance of POLFED with state-of-the-art SIMED code for XXZ and J_1 - J_2 models. Benchmark results are shown in Tab. I and in Tab. II.

The linear scaling of density of states $\rho(0)$ with \mathcal{N} implies that the order of the polynomial spectral transformation $K \propto \mathcal{N}$. Therefore, up to a factor polynomial in L , the computation time of POLFED scales as \mathcal{N}^2 . The total CPU time t_{CPU} for POLFED increases by a factor of ≈ 16 both for XXZ model (Tab. I) and for J_1 - J_2 model (Tab. II) when the system size L increases by 2. Typically, the increase of t_{CPU} is slightly larger when the number N_{cores} of cores (equal to the block size s for POLFED) increases. The memory consumption of POLFED indeed scales as $N_{ev}\mathcal{N}$ up to constant additive factor due to the storing of the Hamiltonian matrix as Tab. I and Tab. II show. The low memory consumption of POLFED allows for calculations on a single node ($N_{cores} \leq 24$ on the supercomputer Prometheus, ACK Cyfronet AGH, Krakow) for both models as long as $L \leq 24$.

The memory consumption of SIMED is dominated by the factors obtained in LU decomposition of the Hamiltonian, it scales as $c(L)\mathcal{N}$ (up to terms polynomial in the system size L). The factor $c(L)$ describes fill-in of the matrix. Tests performed in [35] indicate a phenomenological scaling $c(L) \propto 3^{L/2}$ for XXZ spin chain. This results in total memory needed to store the LU factors to be $\approx 2000GB$ and $14000GB$ respectively for $L = 24$ and $L = 26$. The actual memory usage, due to peaks of allocated/de-allocated memory in the SIMED is significantly higher as shown in Tab. I. The rapid increase of memory consumption with L forces one to use a very large number of nodes in calculations with SIMED, even-

	L	$t_{CPU}[h]$	N_{cores}	$t_W[h]$	$RAM[GB]$	N_{ev}
POLFED	20	3.1	1	3.1	3.9	1000
	22	62.2	4	15.5	21.2	1400
	24	1503	24	62.6	114	2000
	26	19870	24	828	488	2000
SIMED	20	0.5	20	0.026	22	100
	22	20.2	120	0.17	244	100
	24	840	2880	0.23	12288	50
	26	36000	48000	0.75	204800	50

Table I. POLFED vs SIMED for XXZ spin chain: t_{CPU} is total CPU time, N_{cores} is the number of cores used in calculation, t_W is total execution time, RAM is total memory occupation, N_{ev} is the number of obtained eigenpairs in the middle of the spectrum ($\sigma = 0$). Tested on Intel Xeon E5-2680v3 (2.5GHz); SIMED data for $L = 20, 22$ obtained on Intel Ivybridge E5-2680 (2.8GHz), extracted from [35].

	L	$t_{CPU}[h]$	N_{cores}	$t_W[h]$	$RAM[GB]$	N_{ev}
POLFED	20	3.1	1	3.1	0.8	100
	20	3.6	1	3.6	3.9	1000
	22	60.2	1	60.2	3.4	100
	22	63.2	2	31.6	4.5	200
	22	105	8	13.1	21.3	1400
	24	3400	24	142	115	2000
SIMED	20	2.4	36	0.067	70	100
	22	100	468	0.22	1840	100
	22	120	468	0.26	1840	200

Table II. POLFED vs SIMED for J_1 - J_2 spin chain: t_{CPU} is total CPU time, N_{cores} is the number of cores used in calculation, t_W is total execution time, RAM is total memory occupation, N_{ev} is the number of obtained eigenpairs in the middle of the spectrum ($\sigma = 0$). POLFED tested on Intel Xeon E5-2680v3 (2.5GHz); SIMED tested on Intel Xeon Gold 6140 CPU (2.3GHz), data provided by courtesy of F. Alet.

tually making the calculations infeasible, even on large supercomputers. Theoretically, the calculation time of SIMED, dominated by the LU factorization, should be proportional to the number of elements in the factors yielding the scaling of total CPU time $t_{CPU} \propto c(L)\mathcal{N}$. However, as Tab. I shows, t_{CPU} scales more rapidly with system size, increasing approximately 40 times when L increases by 2. Altogether, the system size scaling of t_{CPU} is better for POLFED.

Another aspect of the fill-in phenomenon of SIMED is that it is quite unpredictable. For instance, the coefficient $c(L)$ may change after reordering of the basis. It is, however, clear that the fill-in becomes much more severe as the number N_{nz} of non-zero off-diagonal elements increases. Tab. II shows that the total memory consumption of SIMED for J_1 - J_2 model is increased, in comparison to resources needed for XXZ model, by a factor of ≈ 3.5 and ≈ 7.5 respectively for $L = 20$ and $L = 22$. The total CPU times t_{CPU} for POLFED and

SIMED for J_1 - J_2 model are very similar for $L = 20, 22$. However, the rapidly increasing memory usage of SIMED makes the calculations for $L = 24$ infeasible on present day supercomputers. At the same time, POLFED allows to obtain results for J_1 - J_2 model of size $L = 24$ with resources similar to the XXZ model – such a calculation fits in a single node of a supercomputer.

Another advantage of POLFED is that it allows for a substantial increase of the number of requested eigenvalues, N_{ev} , without a significant increase in the total calculation time. This can be readily understood. When replacing $N_{ev} \rightarrow \alpha N_{ev}$ where $\alpha > 1$, the condition that N_{ev} eigenvalues of $P_\sigma^K(\tilde{H})$ are larger than $p = 0.17$ results in the order of the spectral transformation $K \rightarrow K/\alpha$. Even though the total number of Lanczos iterations needed for the convergence of the algorithm increases by a factor of α , the cost of calculation of a single polynomial spectral transformation decreases α times. The re-orthogonalization performed by POLFED is the only source of increase of total CPU time when $N_{ev} \rightarrow \alpha N_{ev}$. This can be seen in Tab. II as tests for $L = 20, 22$ were performed for few values of N_{ev} . The change of total CPU time with number of requested eigenvalues is more significant for SIMED. For instance, Fig. 6. of [35] shows that increase of N_{ev} from 100 to 1000 results in approximately 6 times larger N_{ev} for XXZ model of size $L = 20$.

Typically, MBL calculations require averaging over disorder realizations. The POLFED allows to find eigenpairs of the disordered spin chains on relatively small number of cores so that the averaging over disorder realizations can be done by performing calculations for many disorder realizations independently at the same time. In contrast, SIMED requires much larger amount of resources. Ultimately, due to smaller total execution times, for XXZ model of sizes $L \leq 24$ SIMED allows to get results for a comparable, but slightly larger number of disorder realizations using a fixed amount of CPU time (assuming than one is able to perform calculations for $L = 24$ simultaneously on 120 nodes of a cluster). For J_1 - J_2 model at system size $L = 20, 22$ POLFED has an advantage. Moreover, while SIMED calculations for J_1 - J_2 model at $L = 24$ are infeasible, they can be readily done by POLFED. The situation is similar for XXZ model at $L = 26$: single SIMED run requires 2000 nodes of a supercomputer, and the calculation is performed in single precision [35] whereas POLFED calculation, in double precision, requires only few nodes of a supercomputer.

Extraction of Thouless time

To extract Thouless time t_{Th} from spectral form factor $K(\tau)$ for system size $L \leq 18$ we use data from full exact diagonalization and follow the procedure outlined in [44]. To this end we calculate the spectral form factor (SFF)

according to its definition

$$K(\tau) = \frac{1}{Z} \left\langle \left| \sum_{j=1}^N g(E_j) e^{-iE_j\tau} \right|^2 \right\rangle. \quad (7)$$

Subsequently, we perform the unfolding, during which the level staircase function $\sigma(\epsilon) = \sum_i \Theta(\epsilon - \epsilon_i)$ (obtained from the set of eigenvalues of the system $\{\epsilon_i\}$ ordered in ascending manner) is separated into smooth and fluctuating parts $\sigma(E) = \bar{\sigma}(E) + \delta\sigma(E)$ and the eigenvalues are mapped via $\epsilon_j \rightarrow E_j = \bar{\sigma}(\epsilon_j)$. As the smooth part $\bar{\sigma}(E)$ we take a polynomial of degree $n_p = 10$ fitted to the level staircase function $\sigma(E)$. To calculate SFF we use $g(\epsilon) \propto \exp(-(\epsilon - \bar{\epsilon})^2 / 2\eta\sigma_\epsilon^2)$, where $\bar{\epsilon}$ denotes the average of the unfolded eigenvalues for given disorder realization ϵ_i , σ_ϵ is the standard deviation of $\{\epsilon_i\}$ and $\eta = 0.3$. This choice of parameters follows precisely [53]. Then, we calculate

$$\Delta K(t/t_H) = \left| \log \left(\frac{K(t/t_H)}{K_{GOE}(\tau = t/t_H)} \right) \right|, \quad (8)$$

where the spectral form factor for GOE is given by

$$K_{GOE}(\tau) = \begin{cases} 2\tau - \tau \ln(1 + 2\tau) & \text{for } \tau \leq 1, \\ 2 - \tau \ln\left(\frac{2\tau+1}{2\tau-1}\right) & \text{for } \tau > 1. \end{cases} \quad (9)$$

The Thouless time t_{Th} is the smallest positive time for which $\Delta K(t/t_H) < a$. We choose the value of cut-off $a = 0.1$.

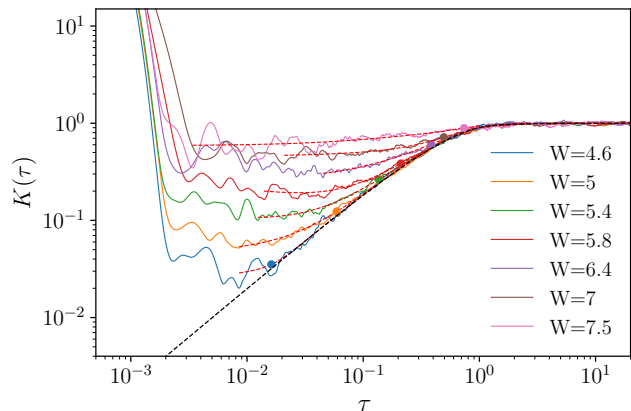


Figure 5. Spectral form factor $K(\tau)$ of J_1 - J_2 model, system size $L = 24$. Black dashed lines shows spectral form factor of GOE, $K_{GOE}(\tau)$. The dashed lines show $K_F(\tau)$ (9) fitted to $K(\tau)$; dots denote the obtained rescaled Thouless time: $\tau_{Th} = t_{Th}/t_H$, where t_H is the Heisenberg time.

For system sizes $L = 20, 22, 24$ we obtain $N_{ev} = 2500$ consecutive eigenvalues from the middle of spectrum. Firstly, we perform the unfolding procedure using fitting the level staircase function with a polynomial of degree

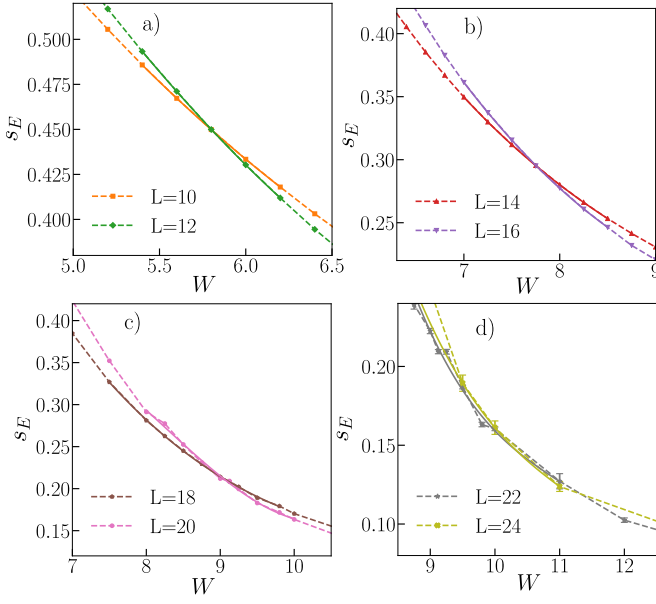


Figure 6. Determination of crossings $s_E(L-1) = s_E(L+1)$ for J_1 - J_2 model. The rescaled entropy s_E , denoted by dashed line, is plotted as a function of disorder strength W for system sizes $L = 10, 12, L = 14, 16, L = 18, 20, L = 22, 24$ respectively on panels a), b), c), d). $s_E(W)$ curves are fitted with polynomials of third degree (shown by solid lines) in vicinity of the crossing point. The crossing points of the polynomials determine $W_E^*(L)$ for $L = 11, 15, 19, 23$.

$n'_p = 3$. Then, we calculate the spectral form factor according to the definition (7) considering only the calculated eigenvalues in the sum. Since the number of disorder realizations we have for the largest system considered ($L = 24$) is only 50, we fit the spectral form factor with the following formula

$$K_F(\tau) = K_{GOE}(\tau) + c_1 \exp(-c_2 \tau^{c_3}), \quad (10)$$

where c_1, c_2, c_3 are fit parameters. The results are shown in Fig. 5. The formula (10) provides very good fits of to the spectral form factor for smaller system sizes ($L \leq 20$) for $\tau \lesssim 0.2\tau_{Th}$. Thus, to extract τ_{Th} for $L = 22, 24$ we use $K_F(\tau)$ in (8).

Fig. 5 illustrates also another aspect of calculation of the Thouless time when not all of the eigenvalues of the system are available. The number of N_{ev} eigenvalues determines the value of $\tau_{N_{ev}}$ below which the spectral form factor rapidly increases. In our case, as can be seen in Fig. 5, $\tau_{N_{ev}} \approx 2 \cdot 10^{-3}$. Once the extracted value of

τ_{Th} is significantly bigger than $\tau_{N_{ev}}$, the value of τ_{Th} is not affected by the fact that $N_{ev} \ll \mathcal{N}$.

Extraction of W^*

To extract the values of $W_E^*(L)$ we plot (for odd L), $s_E(L-1)$ and $s_E(L+1)$ as functions of disorder strength

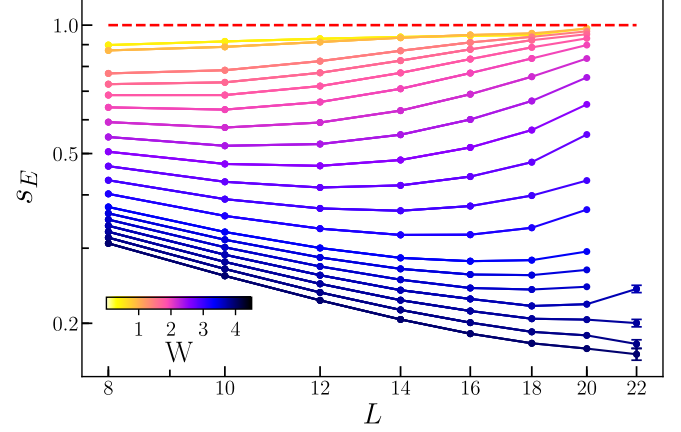


Figure 7. The rescaled entanglement entropy s_E of eigenstates of XXZ model as a function of system size L for disorder strengths $W = 0.5, \dots, 4$ (denoted on the color bar). Dashed lines correspond to ergodic behavior $s_E = 1$.

W , and perform a fit with third order polynomial in the vicinity of the crossing point, examples are shown in Fig. 6. The crossing point of the two polynomials is then the value of $W_E^*(L)$. A similar analysis is performed for even L and data for $s_E(L-2), s_E(L+2)$.

The values of $W_{\bar{r}}^*(L)$ are found in analogous manner from $\bar{r}(L-1)$ and $\bar{r}(L+1)$ ($\bar{r}(L-2)$ and $\bar{r}(L+2)$) as functions of disorder strength W for odd (even) L .

We perform a similar analysis for XXZ model obtaining $W_{E,\bar{r}}^*(L)$ for that system. The scaled entanglement entropy and average gap ratio for XXZ model are shown in Fig. 7 and Fig. 8. The scaled entanglement entropy s_E is obtained when we average S_E over the position of the cut x , over $N_{ev} \leq \min\{\mathcal{N}/100, 2000\}$ eigenstates in the middle of the spectrum ($\sigma = 0$) of XXZ model for system sizes $12 \leq L \leq 22$ (whereas for $L = 8, 10$ we take $N_{ev} = 5$) – similarly as for J_1 - J_2 model. Then, an average over more than 5000, 200 disorder realizations respectively for $L \leq 20, L = 22$ is performed. Eigenvalues corresponding to eigenstates used in calculation of s_E are employed in computation of the average gap ratio \bar{r} .

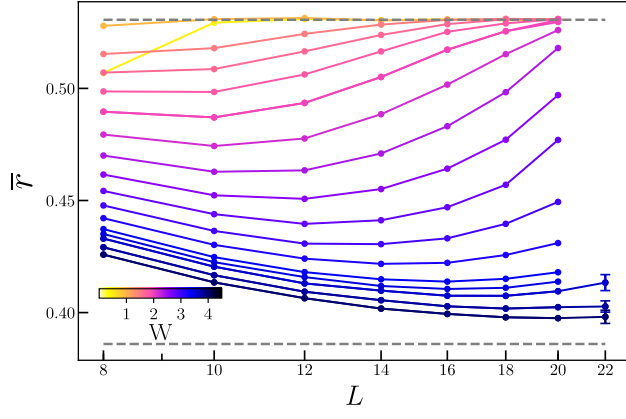


Figure 8. The average gap ratio \bar{s} for XXZ model as a function of system size L for disorder strengths $W = 0.5, \dots, 4$ (denoted on the color bar). Dashed lines correspond to ergodic behavior $s_E = 1$.